ACS Catalysis

Research Article

pubs.acs.org/acscatalysis

Total Hydrogenation of Furfural and 5-Hydroxymethylfurfural over Supported Pd−Ir Alloy Catalyst

Yoshinao Nakagawa,* Kana Takada, Masazumi Tamura, and Keiichi Tomishige*

Department of Applied Chemistry, School of Engineering, Tohoku University, 6-6-07 Aoba, Aramaki, Aoba-ku, Sendai 980-8579, Japan

Supporting Information

ABSTRACT: Hydrogenation of aqueous furfural was conducted with SiO_2-suported palladium-based bimetallic catalysts. The combination of palladium and iridium gave the best performance for the total hydrogenation to tetrahydrofurfuryl alcohol. Higher H_2 pressure and lower reaction temperature were advantageous to suppress side reactions. The synergy between Pd and Ir in the hydrogenation catalysis is most remarkable for substituted furans as substrates. Furfural was first converted into furfuryl alcohol, which was further converted to tetrahydrofurfuryl alcohol. A small amount of tetrahydrofurfural was formed in the first step (~20% selectivity), and the subsequent hydrogenation of tetrahydrofurfural was much slower. The combined yield of tetrahydrofurfuryl alcohol and tetrahydrofurfural reached 98%. The yield of tetrahydrofurfuryl alcohol reached 94% with larger amount of catalyst. Total hydrogenation of 5-hydroxymethylfurfural was also possible using Pd−Ir/SiO_2 catalyst. The performance of Pd−Ir/SiO_2 catalyst was slightly changed by repeated uses, and the used catalyst can be regenerated by calcination and reduction at 573 K. Characterization results showed that Pd−Ir alloy particles with size of ≤4 nm were formed on the catalyst. Addition of Ir much increased the TOF values as compared with Pd/SiO_2 with similar particle size, especially for C═O hydrogenation. One factor of higher activity of Pd−Ir/SiO_2 than Pd/SiO_2 can be the change of adsorption mode: Ir atom on the surface promotes the adsorption at C═O site, whereas the Pd surface strongly interacts with furan ring.

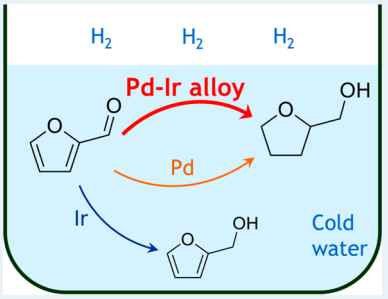

KEYWORDS: *hydrogenation, palladium, iridium, furan, biomass*

1. INTRODUCTION

Biorefinery, the production of fuels or chemicals from biomass, has gained much attention due to the limited fossil fuel resources and global warming issues.[1−7] Oxygen-containing chemicals are more attractive targets than fuels because of the higher market price of chemicals and the lower amount of reducing agent (usually hydrogen) consumed in the conversion process to chemicals.[8−11] Furfural and 5-hydroxymethylfurfural (HMF) are produced from sugars via dehydration and are promising intermediates in biorefinery.[12−18] Furfural and HMF are highly unsaturated compounds, and therefore, hydrogenation is the most important process in the conversion of furfural or HMF.[19,20] Scheme 1 shows the reaction pathways of hydrogenation of furfural and HMF.[19] Hydrogenation of furfural at the aldehyde group and the furan ring gives furfuryl alcohol (FOL) and tetrahydrofurfural, respectively. Further hydrogenation of either compound gives tetrahydrofurfuryl alcohol (THFA). Various side reactions are known such as C−O hydrogenolysis of side-substituents to 2-methylfuran, decarbonylation to furan, and rearrangement to levulinic acid. Further hydrogenation of these byproducts gives more kinds of byproducts. Hydrogenation of HMF gives 2,5-bis(hydroxymethyl)furan (BHF), 5-hydroxymethyltetrahydrofurfural and 2,5-bis(hydroxymethyl)tetrahydrofuran (BHTHF) as products of C−O, furan-ring and total hydrogenation, respectively. Among these products, only FOL has been produced in large scale with Cu−Cr catalyst, and FOL is used in the production of thermostatic resins.[21] Because of the growing interest in HMF, various systems of reduction of HMF into BHF or 2,5-dimethylfuran have been reported.[22−25] On the other hand, THFA and BHTHF can be used as green solvents, because they are degradable, less toxic, and more stable than unsaturated furan compounds.[26] Recently, selective hydrogenolysis systems have been discovered where THFA or BHTHF can be converted into useful straight-chain polyols such as 1,5-pentanediol and 1,6-hexanediol.[27−36] These systems typically use water solvent and Rh or Ir catalysts modified with reducible metal oxide such as ReO_x. Therefore, the importance of total hydrogenation of furfural and HMF has been growing.

Ni catalysts such as Raney Ni are known to be effective in total hydrogenation of furfural and HMF.[37−43] However, Ni catalysts are easily leached in liquid-phase systems,[42] and to make matters worse, dissolved Ni species strongly poison Rh or Ir hydrogenolysis catalysts. The leaching problem can be avoided by application to a gas-phase system;[41] however, very high boiling point of HMF hinders this approach. Ru catalysts have been also reported to be active in the total hydrogenation; however, the selectivity is lower than Ni catalysts, especially

Received: March 8, 2014
Revised: June 16, 2014
Published: July 9, 2014

   dx.doi.org/10.1021/cs500620b | ACS Catal. 2014, 4, 2718−2726

Scheme 1. Reaction Routes of Hydrogenation of Furfural and HMF

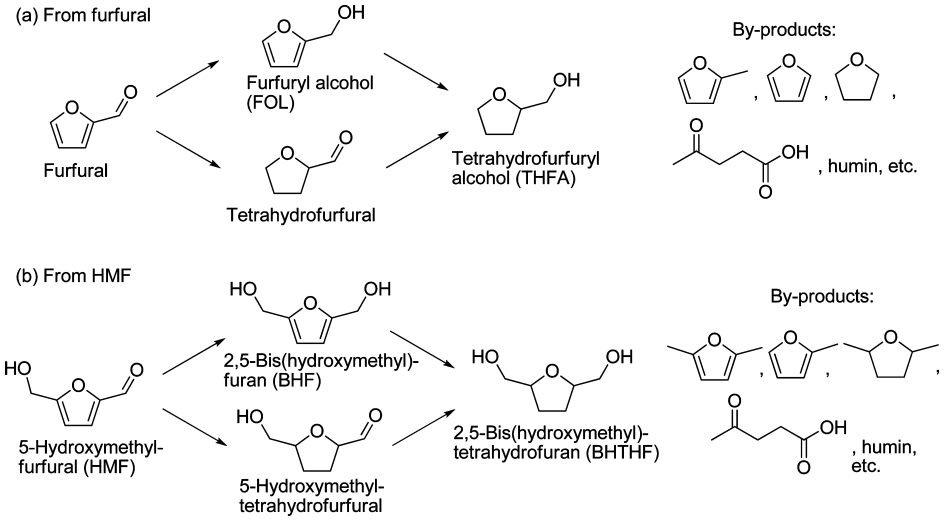

when pure water is used as a solvent.[43,44] Very recently, Biradar et al. reported an effective total hydrogenation system of furfural with Pd/MFI catalyst and isopropyl alcohol solvent.[45] Tuteja et al. reported a hydrogenation/hydrogenolysis system of HMF into 1,6-hexanediol in ethanol with Pd catalyst and formic acid as a hydrogen source.[46] In water solvent, various side reactions such as rearrangement easily proceed during the reduction of furfural or HMF.[19,47−49] Development of stable total hydrogenation catalysts is still a challenging task. A typical method to improve the performance of hydrogenation catalysts is the addition of secondary metal element to active metal (Ni, Cu or noble metal).[50−52] The secondary metal element is usually Sn or first-row transition metal such as Fe. However, this type of bimetallic catalysts is generally effective in selective C═O hydrogenation of unsaturated aldehydes including furfural and HMF, and it is not suitable to total hydrogenation. The selectivity is explained by the presence of cationic species of an additive element that strongly interacts with the C═O group. In addition, these additive elements are easily leached into aqueous media. Therefore, in this study we focused on the combination of noble metals, which are stable in the metallic state in water. We tested various SiO_2-supported bimetallic noble metal catalysts for total hydrogenation of aqueous furfural, and we found that the combination of Pd−Ir was remarkably effective.

2. EXPERIMENTAL SECTION

2.1. Catalyst Preparation. SiO_2 (Fuji silysia G-6; BET surface area 523 $m^2\ g^{-1}$) was used as a support. Catalysts were prepared by impregnating SiO_2 with a mixed aqueous solution of metal precursors. The used precursors were $PdCl_2$ (Kanto Chemical), $RuCl_3{\cdot}nH_2O$ (Kanto Chemical), $RhCl_3$ (Soekawa Chemical), H_2IrCl_6 (Furuya Metals), and H_2PtCl_6 (Kanto Chemical). For monometallic Pd catalyst, the one using $Pd(NH_3)_4(NO_3)_2$ precursor (Sigma-Aldrich) was also prepared (denoted by $Pd/SiO_2(N)$). After impregnation, the catalysts were dried in air at 383 K overnight and then calcined at 773 K for 3 h. The catalyst samples were stored in the calcined form. Reduction was conducted in a glass tube reactor with flowing H_2 for 0.5 h. The reduction temperature was 573 K except in the cases of Pd/SiO_2 and $Pd/SiO_2(N)$ which were reduced at 373 K. The reduced catalysts were passivated with 2% O_2/He at room temperature.

2.2. Activity Tests. Furfural (Wako) was used as received or after distillation. 5-Hydroxymethylfurfural (Sigma-Aldrich) was purified with column chromatography (Merck silica gel 60; methanol/diethyl ether = 2/98).[42] Activity tests were performed in a 190 mL stainless steel autoclave with an inserted glass vessel. An aqueous solution of substrate (0.5 M) was put into the autoclave together with a spinner and reduced catalyst. After sealing the reactors, autoclaves were warmed with a heater (for 313 K reaction) or cooled with a water bath (for 275 or 296 K reaction). After the temperature was stabilized, the gas phase was quickly replaced with hydrogen, and the reaction was started. After an appropriate reaction time, the autoclave contents were transformed to vials, and the catalysts were separated by filtration. The gas phase was also collected in a gas bag. The products were analyzed using a gas chromatograph equipped with FID. A TC-WAX or an InertCap 5 capillary column was used for the separation. Products were also identified using GC-MS (Shimadzu QP 5050), and the details of identification are shown in Supporting Information. Conversions were calculated by the consumption of substrates except in the case of furan hydrogenation where the sum of products was regarded as "conversion". Selectivities were defined as the molar ratio of the product to converted substrate. The kinetic fitting was conducted by minimizing the sum of absolute differences of conversion and selectivities to FOL and THFA in percent between experimental and calculated data. The error range was estimated by changing each parameter while optimizing the other parameter until the sum of absolute differences becomes two times as its minimum value.

2.3. Catalyst Characterization. Temperature-programmed reduction (TPR) with H_2 was performed in a fixed-bed flow reactor. The TPR profile of each sample (~50 mg) was recorded from room temperature to 1073 K at a heating rate of 10 K min^{-1} under a flow of 5% H_2/Ar (30 mL min^{-1}). The amount H_2 in the effluent gas after passing through a frozen acetone trap was monitored with a thermal conductivity detector. XRD patterns of the catalysts were recorded by a Rigaku MiniFlex 600 diffractometer. TEM images were taken with HITACHI HD-2700 or HITACHI HF-2000. EDX analysis was conducted with HITACHI HD-2700. The average

dx.doi.org/10.1021/cs500620b | ACS Catal. 2014, 4, 2718−2726

Table 1. Hydrogenation of Furfural over Various Catalysts[a]

entry	catalyst	Pd loading (wt %)	M/Pd ratio	catalyst amount (mg)	time (h)	conv. (%)	selectivity (%)			
							THFA	FOL	tetrahydro- furfural	others
1	Pd/SiO_2	2		50	1	25	19	69	7	5
2	$Pd/SiO_2(N)$[b]	2		50	1	63	27	33	28	13
3	$Pd–Ir/SiO_2$	2	1	10	1	67	31	47	19	3
4	$Pd–Ru/SiO_2$	2	1	10	1	14	23	49	20	8
5	$Pd–Rh/SiO_2$	2	1	10	1	5.7	13	77	3	7
6	$Pd–Pt/SiO_2$	2	1	10	1	2.5	5	79	<1	16
7	Ir/SiO_2	4[c]		50	1	14	<1	96	<1	4
8	$Pd/SiO_2+Ir/SiO_2$	2	1	25 + 25	1	26	10	85	1	4
9	$Pd–Ir/SiO_2$	3	1/3	10	1	30	27	47	21	5
10	$Pd–Ir/SiO_2$	1	3	10	1	61	19	67	11	3
11	$Pd–Ir/SiO_2$	2	1	10	2	99	63	16	20	2
12	$Pd–Ir/SiO_2$	2	1	10	4	>99	80	<1	18	1
13	$Pd–Ir/SiO_2$	2	1	10	6	>99	80	<1	18	2
14	$Pd–Ir/SiO_2$	2	1	50	6	>99	91	<1	6	4
15	$Pd–Ir/SiO_2$	2	1	150	6	>99	94	<1	1	5

[a]Reaction conditions: Furfural (5 mmol), water (9 g), catalyst (10–150 mg), H_2 (8 MPa), 275 K. [b]Prepared using $Pd(NH_3)_4(NO_3)_2$ precursor. [c]Ir loading amount.

size was calculated by $\sum n_i d_i^3 / \sum n_i d_i^2$ (d_i: particle size, n_i: number of particle with d_i). The amount of CO adsorption was measured in a homemade high-vacuum system by a volumetric method (dead volume: 43 cm^3). The calcined sample (~0.15 g) in the measurement cell was reduced with H_2 at 573 K for 0.5 h and evacuated at 573 K. After cooling to room temperature, CO was introduced and the adsorption amount was measured. The pressure at adsorption equilibrium was about 1 kPa. The physisorption amount of CO on the support was determined by repeating the adsorption measurement after evacuation at room temperature, and the amount was subtracted from that in the first measurement to determine the chemisorption amount. The chemisorption amount was represented as the molar ratio to total noble metal atoms (CO/(Pd + Ir)). FT-IR spectra of adsorbed CO were recorded by a Nicolet 6700 FT-IR with a resolution of 4 cm^{-1} in a transition mode using an in situ cell with CaF_2 windows. The calcined sample was pressed into a self-supporting disk (7 mm diameter, ~30 mg). The sample disk was put into the IR cell connected to the closed circulation system. The samples were reduced with flowing H_2 at 573 K for 0.5 h. After evacuation and cooling, CO (6.7 kPa) was introduced and rested for 1 h. The remaining CO was evacuated, and then FT-IR spectra were recorded. The FT-IR spectra of adsorbed species were obtained by subtracting the spectra of the catalysts before exposing CO.

3. RESULTS AND DISCUSSION

3.1. Optimization of the Catalyst Components. Table 1 shows the results of activity tests of various bimetallic or monometallic noble metal catalysts for hydrogenation of aqueous furfural. Pd was selected as a component because of the high reported hydrogenation activity.[32,39,45,52] We used $PdCl_2$ as a precursor of Pd because precursors of other noble metals were also chlorides. Addition of another noble metal enhanced the catalytic activity (entries 1, 3–6). In particular, addition of Ir gave by far the largest promotion and the highest yield of THFA (entry 3). We also tested Pd/SiO_2 prepared with $Pd(NH_3)_4(NO_3)_2$ as a precursor (denoted by $Pd/SiO_2(N)$; entry 2), because it is known that more dispersed Pd metal particles can be formed from $Pd(NH_3)_4(NO_3)_2$ precursor than from $PdCl_2$.[53] The activity of $Pd–Ir/SiO_2$ catalyst was even higher than that of $Pd/SiO_2(N)$. Monometallic Ir/SiO_2 catalyst showed very low activity and THFA yield (entry 7), showing the synergy between Pd and Ir. Physical mixture of Pd/SiO_2 and Ir/SiO_2 gave almost no enhancing effect in the catalytic performance (entry 8). Various $Pd–Ir/SiO_2$ catalysts were tested with different Ir/Pd ratio and constant total metal amount (entries 3, 9, 10). The catalyst with Ir/Pd = 1 showed the best performance.

There have been limited reports of Pd–Ir bimetallic catalysts. Mahmoud et al. reported that $Pd–Ir/SiO_2$ catalyst prepared by sol–gel method showed higher activity in hydrogenation of cinnamaldehyde in toluene than Pd/SiO_2 with the same Pd amount.[54] However, the increase of activity was rather small (<1.3 times) when compared on the basis of the Pd + Ir amount. The promotion by Ir addition in our system was more drastic than this literature system. Rocha et al. reported Pd–Ir catalysts supported on H–Y zeolite for hydrogenation of tetralin to decaline with fixed-bed flow system at high temperature (523 K).[55] The catalyst with the molar ratio of Ir/Pd = 1 showed the highest activity in catalysts with the same Pd + Ir amount, although the difference from monometallic Pd catalyst was very small. López-De Jesús et al. reported the catalysis of $Pd–Ir/\gamma\text{-}Al_2O_3$ for hydrogenation of benzonitrile to benzylamine, dibenzylamine, or toluene in ethanol.[56] The catalyst with the ratio of Ir/Pd = 1 showed higher activity, especially for the formation of benzylamine, than those with Ir/Pd = 4 or 1/4. However, the reported TOF of $Pd–Ir/\gamma\text{-}Al_2O_3$ (Ir/Pd = 1) based on the surface atoms was lower to that of $Pd/\gamma\text{-}Al_2O_3$. Ziasi-azad et al. have recently reported $Pd–Ir/\gamma\text{-}Al_2O_3$ catalysts with homogeneous alloy or core(Pd)-shell(Ir) structure and the application to ring-opening reaction of Indane.[57] Pd works only as an inert surface diluting metal in this ring-opening reaction. Above all, the remarkable synergy between Pd and Ir like this furfural hydrogenation has not been reported.

3.2. Performance of $Pd–Ir/SiO_2$ (Pd/Ir = 1). The time course of hydrogenation of furfural over $Pd–Ir/SiO_2$ (Pd/Ir = 1) is also shown in Table 1. FOL was the main product at shorter reaction time, and later FOL was converted to THFA, similarly to other reported systems of furfural hydrogenation to THFA.[41–45] Smaller amount of tetrahydrofurfural was also

dx.doi.org/10.1021/cs500620b | ACS Catal. 2014, 4, 2718–2726

Table 2. Hydrogenation of HMF over Pd−Ir/SiO_2 Catalyst[a]

				selectivity (%)			
entry	catalyst amount (mg)	time (h)	conv. (%)	BHTHF	BHF	5-hydroxymethyl- tetrahydrofurfural	others
1	10	1	>99	85	<1	14	1
2	150	4	>99	95	<1	1	4

[a]Reaction conditions: HMF (5 mmol), water (9 g), Pd−Ir/SiO_2 (Pd 2 wt %, Ir/Pd = 1) 10 or 150 mg, H_2 (8 MPa), 275 K.

formed, and the hydrogenation of tetrahydrofurfural was relatively slow. At 4 h, FOL was totally converted, and the yield of THFA reached 80% (entry 14). At that time, the yield of tetrahydrofurfural was 18%. Higher yield of THFA can be obtained with larger amount of catalyst, which effectively increases reaction progress at the same reaction time. With 0.15 g catalyst (15 times larger amount), 94% yield of THFA was obtained (entry 15).

This catalytic system was further applied to HMF hydrogenation. The results were similar to those for furfural hydrogenation (Table 2). Mixture of BHTHF and 5-hydroxymethyltetrahydrofurfural was obtained in short reaction time (entry 1), and high yield of BHTHF (95%) was obtained with larger amount of catalyst (entry 2). The reactivity of HMF was higher than furfural over this Pd−Ir/SiO_2 catalyst. This is in contrast to the case of Ni−Pd/SiO_2 catalyst where the reactivity of HMF is minimally higher than furfural.[42]

The effect of reaction conditions on the catalytic performance are shown in Figure 1. The activity was increased with increasing H_2 pressure for both Pd−Ir/SiO_2 and monometallic catalysts. Higher H_2 pressure was also advantageous in terms of selectivity: byproducts from other reactions than hydrogenation were suppressed by higher H_2 pressure. The substrate concentration had little effect in the catalysis. The reaction temperature affected the selectivity as well as activity: higher reaction temperature promoted side reactions. The increase of activity by higher reaction temperature was relatively small, especially for the Ir/SiO_2 catalyst. After all, higher H_2 pressure and lower reaction temperature are advantageous to this hydrogenation system.

The reusability of Pd−Ir/SiO_2 was tested (Figure 2). First, the used catalyst was collected by centrifugation, and reused without reactivation. In this case, the selectivity was gradually changed by subsequent reuse: the hydrogenation activity of the furan ring was decreased. The activity during the third run was slightly lower than that of fresh catalyst. After three uses, the catalyst was calcined at 573 K and then reduced again at 573 K. The regenerated catalyst showed almost the same performance as fresh one. The used catalyst might be poisoned by some byproducts such as polymer or CO, which can be removed by calcination.

3.3. Catalyst Characterization. The TPR profile of calcined Pd−Ir/SiO_2 (Pd/Ir = 1) is shown in Figure 3a. Consumption signal was observed between 350 and 550 K, and the molar ratio of consumed H_2 to Ir was 1.2. This value was smaller than the value for the reduction of IrO_2,[58,59] and a part of Ir in addition to Pd was already reduced at room temperature. A small desorption peak was observed at 350 K, similarly to the pattern of Pd/SiO_2 (Figure 3b), also indicating that metallic phase was already formed at room temperature. The consumption signal of Pd−Ir/SiO_2 (peak top: 460 K) was slightly shifted to lower temperature than Ir/SiO_2 (peak top: 510 K; Figure 3e[59]), indicating that reduction of Ir was promoted by addition of Pd. The TPR profiles of catalysts after reduction and passivation showed no apparent H_2 consumption

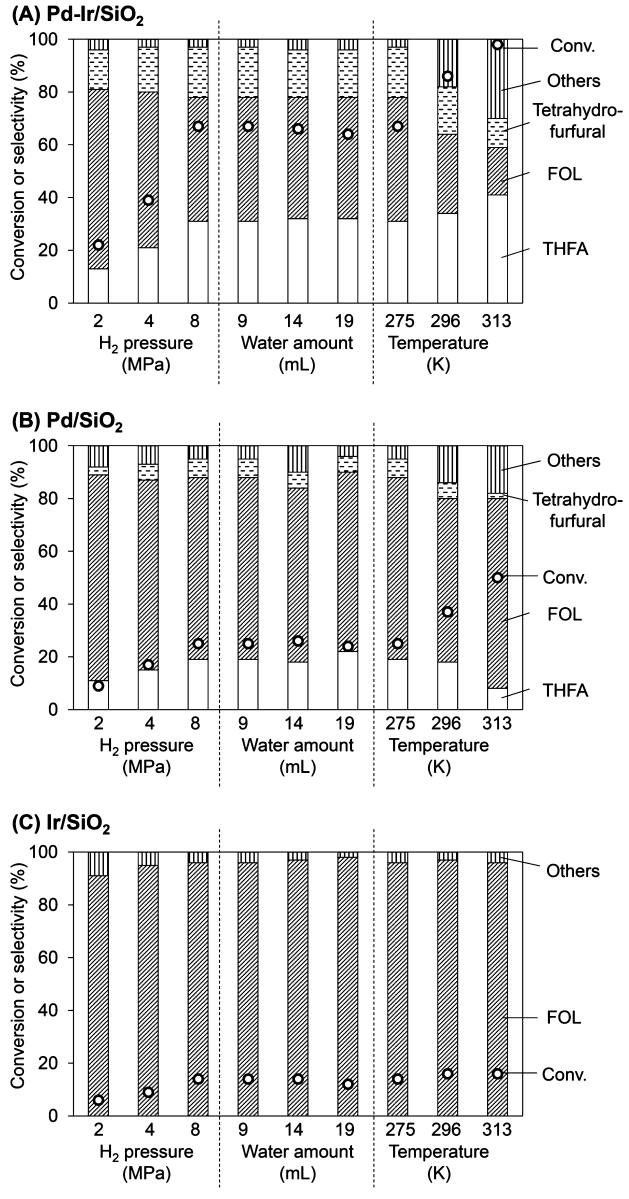

Figure 1. Hydrogenation of furfural in various reaction conditions. Standard reaction conditions: catalyst (10 mg for Pd−Ir/SiO_2 (Ir/Pd = 1), 50 mg for Pd/SiO_2 or Ir/SiO_2), furfural (5 mmol), water (9 g), H_2 (8 MPa), 275 K, 1 h.

signal above room temperature (Figure 3c,d), suggesting that the catalysts in the reaction media were totally reduced. The XRD patterns of catalysts are shown in Figure 4. Reduced monometallic catalysts (Pd/SiO_2, Pd/SiO_2(N), and Ir/SiO_2) clearly showed the peaks of the metallic phase in addition to the broad peak of SiO_2 support (~22°). The particle size calculated by the width of the XRD peak of (111) reflection at around 40° was 4 nm for both Pd/SiO_2(N) and Ir/SiO_2 and 7 nm for Pd/SiO_2. Reduced Pd−Ir/SiO_2 at 573 K, which was used for

dx.doi.org/10.1021/cs500620b | ACS Catal. 2014, 4, 2718−2726

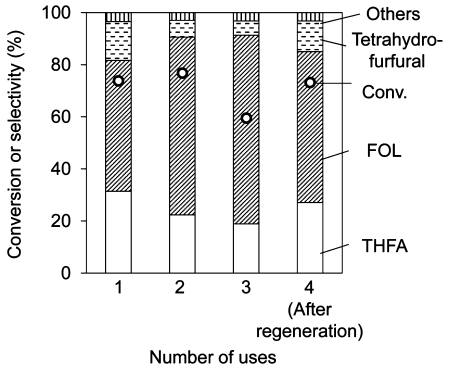

Figure 2. Reuses of Pd–Ir/SiO_2 catalyst. Reaction conditions: Pd–Ir/SiO_2 (Ir/Pd = 1; 10 mg), furfural (5 mmol), water (9 g), H_2 (8 MPa), 275 K, 1 h. The catalyst after the third run was calcined at 573 K for 3 h and then reduced with H_2 at 573 K for 0.5 h before the fourth run.

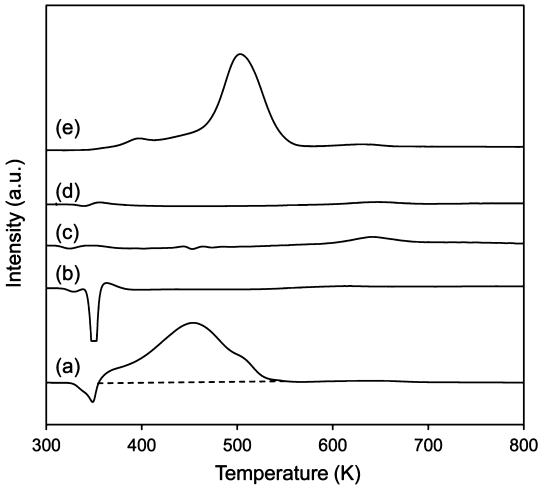

Figure 3. TPR profiles of catalysts. (a) Pd–Ir/SiO_2 (Ir/Pd = 1), (b) Pd/SiO_2, (c) Pd–Ir/SiO_2 (Ir/Pd = 1) after reduction and passivation, (d) Ir/SiO_2 after reduction and passivation, and (e) Ir/SiO_2. The broken line is the baseline for integration. The pattern of (e) is reproduced from ref 59. Copyright 2011 Elsevier.

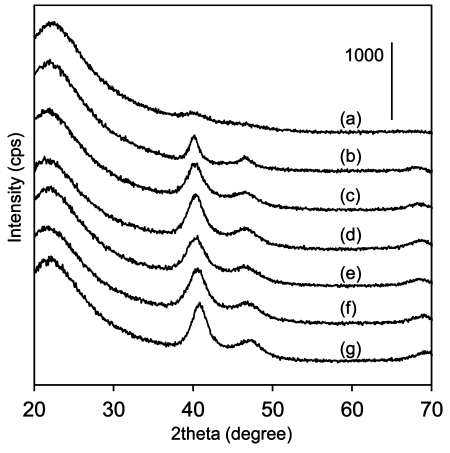

Figure 4. XRD patterns of reduced catalysts. (a) Pd/SiO_2(N), (b) Pd/SiO_2, (c) Pd–Ir/SiO_2 (Ir/Pd = 1/3), (d) Pd–Ir/SiO_2 (Ir/Pd = 1), (e) Pd–Ir/SiO_2 (Ir/Pd = 1) after reaction, (f) Pd–Ir/SiO_2 (Ir/Pd = 3), (g) Ir/SiO_2.

catalytic reaction, showed the peaks located between those of Pd metal and Ir metal. In particular, the catalyst with Ir/Pd = 1 showed the (111) peak (40.4°) at the midmost positions between the simple substances (40.1 and 40.7°). The pattern suggests the formation of alloy phase; however, the overlap of two different monometallic phases cannot be ruled out. Figure 5 show the TEM image of reduced Pd–Ir/SiO_2 (Ir/Pd = 1).

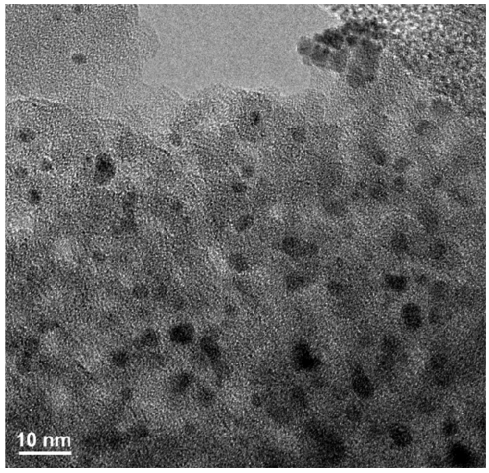

Figure 5. TEM image of reduced Pd–Ir/SiO_2 (Ir/Pd = 1).

Metal nanoparticles were observed with narrow distribution of size, and the average size was 3.4 nm. The particle size was similar to those of Pd/SiO_2(N) (TEM images of Pd/SiO_2 and Pd/SiO_2(N) are shown in Supporting Information) and Ir/SiO_2 (3.6 nm).[59] The EDX analysis was conducted to determine the distribution of each metal. Although the element distribution in one particle could not be determined because of the small particle size, the element distribution among particles was determined to be narrow and centered at the ratio of the whole sample (Pd/Ir = 1:1; Figure 6), showing the formation

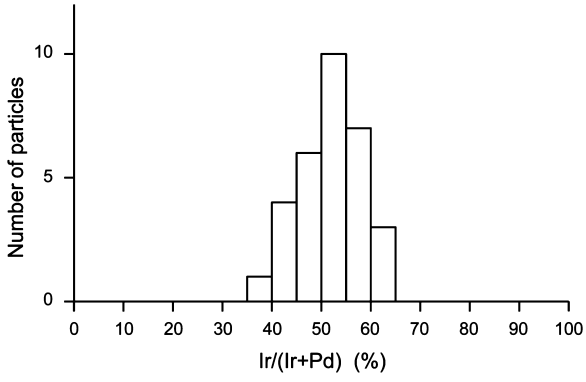

Figure 6. EDX analysis of particles on reduced Pd–Ir/SiO_2 (Ir/Pd = 1).

of bimetallic particles. The particle size was also calculated by the width of the XRD peak of (111) reflection at around 40° (Figure 4d). The calculated value was 3.5 nm. The particle size of bimetallic particles calculated from XRD line width is generally underestimated by the broadening derived from the heterogeneity of alloy compositions. This agreement in particle sizes determined by TEM and XRD suggests the formation of uniform Pd–Ir alloy particles. The XRD peak positions of Pd–Ir/SiO_2 (Ir/Pd = 1) also supports the formation of uniform alloy. We measured the FT-IR spectra of adsorbed CO on the reduced catalysts in order to see the property of metal surface

dx.doi.org/10.1021/cs500620b | ACS Catal. 2014, 4, 2718–2726

(Figure 7). On Ir/SiO_2 catalyst, one strong peak at 2079 cm^{-1} assignable to linear CO on Ir was observed. On the $Pd–Ir/SiO_2$

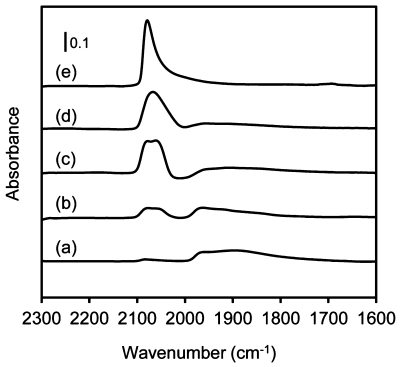

Figure 7. FT-IR spectra of adsorbed CO on the catalysts. (a) $Pd/SiO_2(N)$, (b) $Pd–Ir/SiO_2$ (Ir/Pd = 1/3), (c) $Pd–Ir/SiO_2$ (Ir/Pd = 1), (d) $Pd–Ir/SiO_2$ (Ir/Pd = 3), (e) Ir/SiO_2.

catalyst with high Ir/Pd ratio (Ir/Pd = 3), the peak was slightly shifted to lower wavenumber (2067 cm^{-1}). With decreasing Ir/Pd ratio, the signal for linear CO was splitted into two peaks, and one broad signal below 2000 cm^{-1} appeared. The latter signal can be assigned to bridge CO on Pd, and this type of signal was the main band for monometallic $Pd/SiO_2(N)$ catalyst (Figure 7a). The presence of a small amount of bridge CO on the bimetallic Pd–Ir particles means the presence of Pd atom on the surface as well as Ir. It should be noted that metallic Pd was formed at much lower temperature than metallic Ir and that the number of atoms on the particle surface was smaller than that of the total Ir atoms. Therefore, a portion of the Ir^0 atoms formed during the reduction was moved into the inside of particles. The signal for linear CO on Pd particle in $Pd/SiO_2(N)$ was located at 2083 cm^{-1}, and in the literature, the signal for linear CO on Pd surface is reported to be located at around 2090 cm^{-1}.[60] These wavenumber values are larger than that of linear CO on Ir. Therefore, the peaks with lower and higher wavenumber for linear CO on bimetallic catalyst (2062 and 2079 cm^{-1} for Ir/Pd = 1 sample) can be tentatively assigned to CO on Ir and Pd, respectively. Increasing amount of linear CO on Pd by alloy formation has been observed for other Pd–M systems such as Pd–Ag,[61] and this phenomenon can be explained by decrease of $Pd_{surface}$—$Pd_{surface}$ bonds. Anyway, the spectral patterns of CO on $Pd–Ir/SiO_2$ were different from the simple sum of those on Pd metal and Ir metal, supporting the formation of Pd–Ir alloy.

Above all results show that reduced $Pd–Ir/SiO_2$ (Ir/Pd = 1) contains Pd–Ir alloy particles with the size of ≤4 nm. The CO adsorption amount of $Pd/SiO_2(N)$, Ir/SiO_2, and $Pd–Ir/SiO_2$ (Ir/Pd = 1) was similar in the ratio to total metal atoms: CO/(Pd + Ir) = 0.19, 0.17, and 0.16, respectively. The higher activity of $Pd–Ir/SiO_2$ than Pd/SiO_2 (and $Pd/SiO_2(N)$) and Ir/SiO_2 indicates that Pd–Ir alloy phase has high catalytic activity than Pd or Ir monometallic phases.

In the literature, limited characterizations have been reported for Pd–Ir catalysts except size-related techniques such as TEM and adsorption amounts.[54−56] On the other hand, Ziaki-azad et al. reported the formation of Pd–Ir random alloy particles prepared by reduction of mixed solution of $PdCl_2$ and $IrCl_3$ with refluxing ethanol.[57] They characterized the particles with various techniques such as XPS, XANES, and ion-scattering spectroscopy. However, both literature data and our data cannot strictly decide whether completely uniform alloy phase was formed or not; that is, we do not exclude the possibility that heterogeneity of compositions exists in each particle. The decision will be another work.

The used $Pd–Ir/SiO_2$ catalyst (Ir/Pd = 1) was also characterized with XRD (Figure 4e) and TEM (Figure S2 in Supporting Information). The obtained data was essentially identical to the fresh, unused catalyst, also confirming the stability of the catalyst.

3.4. Reaction Mechanism. Table 3 shows the comparison of reactivity between furfural, FOL, and furan over $Pd–Ir/SiO_2$, Ir/SiO_2, Pd/SiO_2, and $Pd/SiO_2(N)$. $Pd–Ir/SiO_2$ showed higher activity than Ir/SiO_2 for all these substrates. However, the difference of activity between $Pd–Ir/SiO_2$ and monometallic Pd catalyst was varied with substrates. $Pd–Ir/SiO_2$ showed higher activity than Pd/SiO_2 and $Pd/SiO_2(N)$ in furfural hydrogenation, as discussed in section 3.1. The promoting effect of Ir addition was smaller in FOL hydro-

Table 3. Hydrogenation of Furanic Compounds over Pd/SiO_2, $Pd–Ir/SiO_2$ (Ir/Pd = 1), and Ir/SiO_2[a]

entry	catalyst	catalyst amount (mg)	conv. (%)	products (selectivity (%))
furfural hydrogenation (furfural = 5 mmol)				
1	Pd/SiO_2	50	25	THFA (19), FOL (69), tetrahydrofurfural (7)
2	$Pd/SiO_2(N)$	50	63	THFA (27), FOL (33), tetrahydrofurfural (28)
3	$Pd–Ir/SiO_2$	10	67	THFA (31), FOL (47), tetrahydrofurfural (19)
4	Ir/SiO_2	50	14	FOL (96)
5[b]	Ir/SiO_2	50	94	FOL (99)
FOL hydrogenation (FOL = 5 mmol)				
6	Pd/SiO_2	50	11	THFA (99)
7	$Pd/SiO_2(N)$	50	84	THFA (96)
8	$Pd–Ir/SiO_2$	10	46	THFA (99)
9	Ir/SiO_2	50	2	THFA (64)
furan hydrogenation (furan = 50 mmol)				
10	Pd/SiO_2	50	3.1	tetrahydrofuran (99)
11	$Pd/SiO_2(N)$	10	5.8	tetrahydrofuran (99)
12	$Pd–Ir/SiO_2$	10	5.8	tetrahydrofuran (99)
13	Ir/SiO_2	50	0.2	tetrahydrofuran (39), 1-butanol (61)

[a]Other conditions: water (9 g), H_2 (8 MPa), 275 K, 1 h. [b]313 K, 24 h.

dx.doi.org/10.1021/cs500620b | ACS Catal. 2014, 4, 2718−2726

Table 4. Kinetic Parameters in the Hydrogenation of Furfural under 8 MPa H_2 at 275 K

catalyst	Pd–Ir/SiO_2 (Ir/Pd = 1)	Pd/SiO_2	Pd/SiO_2(N)	Ir/SiO_2
S_{FOL} (%)	78	88	60	96
k_1 (mmol g_{cat}^{-1} min^{-1})[a]	11 (9–13)	0.7 (0.3–1.8)	1.4 (1.2–1.6)	0.2
k_2 (mmol g_{cat}^{-1} min^{-1})	3.9	0.18	1.4	0.03
$K_{furfural}/K_{FOL}$[a]	0.5 (0.36–0.6)	0.3 (0.1–0.7)	1.0 (0.7–1.4)	≫1
total metal (mmol g_{cat}^{-1})	0.38	0.19	0.19	0.21
particle size (nm)[b]	3.5	7	4.1	3.6[c]
CO adsorption (CO/(Ir + Pd))	0.16	0.04	0.19	0.23[c]
$TOF_{C=O}$ (10^4 h^{-1})[d]	1.1 (0.9–1.3)	0.6 (0.2–1.4)	0.2 (0.20–0.27)	0.03
$TOF_{C=C}$ (10^4 h^{-1})[e]	0.4	0.1	0.2	0.005

[a]Determined by fitting. The numbers in parentheses are the error range (see section 2.2 for the determination of the error range in the fitting). [b]Determined by XRD. [c]Ref 59. [d]Calculated by $(k_1)/[(\text{total metal})\{CO/(Ir + Pd)\}]$. The numbers in parentheses are the error range derived from fitting. [e]Calculated by $(k_2)/[(\text{total metal})\{CO/(Ir + Pd)\}]$.

genation. For furan, the activities of Pd–Ir/SiO_2 and Pd/SiO_2(N) was quite similar.

When both furfural and FOL exist in the reaction media, the relative reactivity can be changed by the relative adsorption ability of these substrates on the catalyst surface. We analyzed the selectivity change in the time course based on Langmuir–Hinshelwood kinetic model. Different activation sites for organic molecules and hydrogen were assumed because of the positive reaction order with respect to H_2 pressure and low, not negative reaction order with respect to furfural concentration (Figure 1). We have used similar model for the kinetic analysis for gas-phase furfural hydrogenation over Ni/SiO_2.[41] We considered two reactions: furfural hydrogenation to FOL (eq 1) and FOL hydrogenation to THFA (eq 2).

$$\text{furfural} + H_2 \rightarrow \text{FOL} + \text{other products (tetrahydrofurfural + others)} \quad (1)$$

$$\text{FOL} + 2H_2 \rightarrow \text{THFA} \quad (2)$$

On the basis of the model, the following equations for concentration changes can be derived.

$$d[\text{furfural}]/dt = -(W/V)k_1K_{furfural}[\text{furfural}]/(1 + K_{furfural}[\text{furfural}] + K_{FOL}[FOL]) \quad (3)$$

$$d[FOL]/dt = (W/V)\{k_1S_{FOL}[\text{furfural}]/(1 + K_{furfural}[\text{furfural}] + K_{FOL}[FOL]) - k_2K_{FOL}[FOL]/(1 + K_{furfural}[\text{furfural}] + K_{FOL}[FOL])\} \quad (4)$$

$$d[THFA]/dt = (W/V)k_2K_{FOL}[FOL]/(1 + K_{furfural}[\text{furfural}] + K_{FOL}[FOL]) \quad (5)$$

Here, k_1 and k_2 are the rate constants of furfural conversion and FOL hydrogenation, respectively. W and V means the catalyst weight and volume of reaction solution, respectively. The term of the number of active sites per unit catalyst weight is included in k_1 and k_2. The term of hydrogen pressure is also included to these rate constants, because hydrogen pressure was almost constant (8 MPa) in these reaction tests. $K_{furfural}$ and K_{FOL} are the equilibrium constant of adsorption of furfural and FOL, respectively. S_{FOL} and $(1 - S_{FOL})$ are the selectivities to FOL and (tetrahydrofurfural + others), respectively, in the first step of the conversion of furfural.

The selectivity to (tetrahydrofurfural + others) of the total system will be constant $(1 - S_{FOL})$ during the time course in this model, and therefore, S_{FOL} can be obtained from the data in Table 1. On the basis of the low reaction order with respect to furfural concentration (Figure 1), the $K_{furfural}$ value should be large ($K_{furfural}$[furfural] ≫ 1). The values of k_2 can be obtained from the FOL hydrogenation data in Table 3, entries 6–9 on the assumption that K_{FOL} value is also large: K_{FOL}[FOL] ≫ 1 and [furfural] = 0; eq 4 is simplified into $d[FOL]/dt = -(W/V)k_2$. We calculated k_1 and $K_{furfural}/K_{FOL}$ values by fitting to the conversion and selectivity patterns (Table 4 and Figure 8).

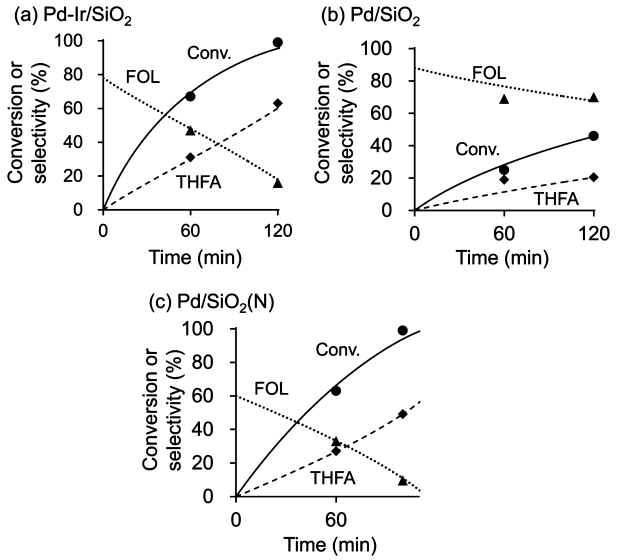

Figure 8. Fitted profiles of furfural hydrogenation. Markers: experimental data (Table 1 and additional data for longer reaction time); lines: calculated curves using kinetic parameters shown in Table 4

For Pd/SiO_2 with large crystal size, low $K_{furfural}/K_{FOL}$ value (~0.3) was calculated, showing that FOL is adsorbed on Pd surface considerably stronger than furfural. The stronger adsorption of FOL than furfural on Pd(111) surface has been already reported.[62] According to the DFT calculations, all the carbon atoms in the furan ring of furfural or FOL are bonded to surface Pd atoms.[63] The electron-withdrawing nature of the carbonyl group may weaken the adsorption of the furan ring of furfural on Pd.

On the other hand, Pd/SiO_2(N) with smaller particle size showed larger $K_{furfural}/K_{FOL}$ ratio (1.0) than Pd/SiO_2. The difference between k_1 values of these monometallic Pd catalysts was rather small, and, because of the difference of the number of surface atoms, the TOF value for C=O hydrogenation of Pd/SiO_2(N) was not higher than that of Pd/SiO_2. The lower

dx.doi.org/10.1021/cs500620b | ACS Catal. 2014, 4, 2718–2726

activity of Pd/SiO_2 than $Pd/SiO_2(N)$ in furfural hydrogenation was due to the fewer active sites and the blocking of active site by produced FOL. In contrast, k_2 and TOF for FOL hydrogenation of $Pd/SiO_2(N)$ were surely larger than those of Pd/SiO_2. The high activity of $Pd/SiO_2(N)$ in furan ring hydrogenation was also observed in hydrogenation of furan itself (Table 3, entries 10 and 11). Hydrogenation activity is known to be strongly related to the adsorption structure. The sites directly bonded to the surface metal atoms are generally reacted. However, too strong adsorption can rather decrease the reactivity. The high activity of $Pd/SiO_2(N)$ in furan ring hydrogenation may be due to weaker adsorption of furan ring.

In the case of Ir/SiO_2, hydrogenation of FOL to THFA took place to some extent when FOL alone was used as substrate, whereas THFA was not produced at all in the hydrogenation of furfural even at high conversion. These data mean that $K_{furfural}/K_{FOL}$ was very large. Similar weaker adsorption of FOL has been reported for Cu and Ni surfaces, where the adsorption with only the C=O site of furfural is proposed.[41,64,65] The reactivity of adsorbed species on Ir (k_1, k_2, and TOF values) was much lower than that on Pd. Reyes et al. reported that Ir/TiO_2 adsorbs crotonaldehyde at the positively charged Ir center as [—C=O···surface] complex.[66]

In the case of $Pd–Ir/SiO_2$, a moderate value (0.5) of $K_{furfural}/K_{FOL}$ ratio and very large k_1 (or TOF for C=O hydrogenation) was calculated. The k_2 value or TOF for FOL hydrogenation was also larger than those of monometallic Pd catalysts. In light of the above considerations, it is believed that the addition of Ir may promote the adsorption of C=O site of furfural and weaken the adsorption of furan ring. The schematic picture of furfural adsorption on the catalysts is shown in Figure 9. Both

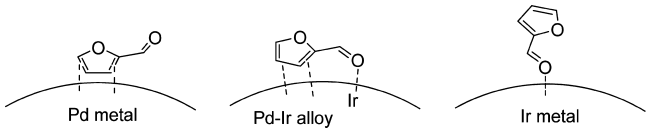

Figure 9. Proposed adsorption structure of furfural on catalyst surface.

of these effects on adsorption can increase the reaction rate: the adsorption of C=O site can increase k_1, and the weakened adsorption of furan ring can increase k_2. The particle size may also affect the adsorption strength of furan ring and k_2 value.

4. CONCLUSIONS

Simple coimpregnation of Pd and Ir on SiO_2 gives Pd–Ir alloy particles after reduction with H_2 at 573 K. The Pd–Ir alloy particles show very high catalytic activity in total hydrogenation of furfural and 5-hydroxymethylfurfural in water. The remarkable synergy between Pd and Ir is specific to hydrogenation of substituted furans. High hydrogen pressure and low reaction temperature are advantageous to obtain good yields. The surface of Pd–Ir alloy catalyst has much higher TOF than monometallic Pd catalyst with similar particle size, especially for C=O hydrogenation of furfural. Monometallic Ir catalyst has much lower activity or TOF for both C=O hydrogenation of furfural and C=C hydrogenation of furan ring than Pd and Pd–Ir catalysts. In addition, in the presence of furfural, the hydrogenation of furfuryl alcohol over Ir is totally suppressed, suggesting the strong adsorption of C=O group on surface Ir atom. The adsorption of C=O group on surface Ir atom might also exist in Pd–Ir alloy catalyst, which can cause the higher C=O hydrogenation activity than Pd catalysts.

ASSOCIATED CONTENT

Supporting Information

Details of identification of products, TEM images of Pd/SiO_2, $Pd/SiO_2(N)$, and used $Pd–Ir/SiO_2$ (Ir/Pd = 1), and the histograms of size distributions. This material is available free of charge via the Internet at http://pubs.acs.org.

AUTHOR INFORMATION

Corresponding Authors

*E-mail: yoshinao@erec.che.tohoku.ac.jp. Fax/Tel.: +81-22-795-7215.

*E-mail: tomi@erec.che.tohoku.ac.jp. Fax/Tel.: +81-22-795-7214.

Notes

The authors declare no competing financial interest.

ACKNOWLEDGMENTS

This work was in part supported by the Cabinet Office, Government of Japan through it is "Funding Program for Next Generation World-Leading Researchers". We thank Prof. T. Kizuka (University of Tsukuba) and Technical Division, School of Engineering, Tohoku University for TEM observation.

REFERENCES

(1) Corma, A.; Ibbora, S.; Velty, A. *Chem. Rev.* **2007**, *107*, 2411–2502.
(2) Chheda, J. N.; Hubewr, G. W.; Dumesic, J. A. *Angew. Chem., Int. Ed.* **2007**, *46*, 7164–7183.
(3) Fernando, S.; Adhikari, S.; Chandrapal, C.; Murali, N. *Energy Fuels* **2006**, *20*, 1727–1737.
(4) Ragauskas, A. J.; Williams, C. K.; Davison, B. H.; Britovsek, G.; Cairney, J.; Eckert, C. A.; Frederick, W. J., Jr.; Hallett, J. P.; Leak, D. J.; Liotta, C. L.; Mielenz, J. R.; Murphy, R.; Templer, R.; Tschaplinski, T. *Science* **2006**, *311*, 484–489.
(5) Demirbas, M. F.; Balat, M. *Energy Convers. Manage.* **2006**, *47*, 2371–2381.
(6) Marshall, A.-L.; Alaimo, P. J. *Chem.—Eur. J.* **2010**, *16*, 4970–4980.
(7) Besson, M.; Gallezot, P.; Pinel, C. *Chem. Rev.* **2014**, *114*, 1827–1870.
(8) Schlaf, M. *Dalton Trans.* **2006**, 4645–4653.
(9) Rinaldi, R.; Schüth, F. *Energy Environ. Sci.* **2009**, *2*, 610–626.
(10) Kobayashi, H.; Ohta, H.; Fukuoka, A. *Catal. Sci. Technol.* **2012**, *2*, 869–883.
(11) Ruppert, A. M.; Weinberg, K.; Palkovits, R. *Angew. Chem., Int. Ed.* **2012**, *51*, 2564–2601.
(12) Tong, X.; Ma, Yang; Li, Y. *Appl. Catal., A* **2010**, *385*, 1–13.
(13) Zakrzewska, M. E.; Bogel-Łukasik, E.; Bogel-Łukasik, R. *Chem. Rev.* **2011**, *111*, 397–417.
(14) Karinen, R.; Vilonen, K.; Niemelä, M. *ChemSusChem* **2011**, *4*, 1002–1016.
(15) Lange, J.-P.; van der Heide, E.; van Buijtenen, J.; Price, R. *ChemSusChem* **2012**, *5*, 150–166.
(16) Moreau, C.; Belgacem, M. N.; Gandini, A. *Top. Catal.* **2004**, *27*, 11–30.
(17) Lewkowski, J. *Arkivoc* **2001**, *1*, 17–54.
(18) Van Putten, R.-J.; van der Waal, J. C.; de Jong, E.; Rasrendra, C. B.; Heeres, H. J.; de Vries, J. G. *Chem. Rev.* **2013**, *113*, 1499–1597.
(19) Nakagawa, Y.; Tamura, M.; Tomishige, K. *ACS Catal.* **2013**, *3*, 2655–2668.
(20) Medlin, J. W. *ACS Catal.* **2011**, *1*, 1284–1297.
(21) Wu, J.; Shen, Y.; Liu, C.; Wang, H.; Geng, C.; Zhang, Z. *Catal. Commun.* **2005**, *6*, 633–637.
(22) Tamura, M.; Tokonami, K.; Nakagawa, Y.; Tomishige, K. *Chem. Commun.* **2013**, *49*, 7034–7036.

(23) Ohyama, J.; Esaki, A.; Yamamoto, Y.; Arai, S.; Satsuma, A. *RSC Adv.* **2013**, *3*, 1033−1036.
(24) Román-Leshkov, Y.; Barrett, C. J.; Liu, Z. Y.; Dumesic, J. A. *Nature* **2007**, *447*, 982−986.
(25) Nishimura, S.; Ikeda, N.; Ebitani, K. *Catal. Today* **2014**, *232*, 89−98.
(26) Chen, X.; Sun, W.; Xiao, N.; Yan, Y.; Liu, S. *Chem. Eng. J.* **2007**, *126*, 5−11.
(27) Koso, S.; Furikado, I.; Shimao, A.; Miyazawa, T.; Kunimori, K.; Tomishige, K. *Chem. Commun.* **2009**, 2035−2037.
(28) Koso, S.; Ueda, N.; Shinmi, Y.; Okumura, K.; Kizuka, T.; Tomishige, K. *J. Catal.* **2009**, *267*, 89−92.
(29) Chen, K.; Koso, S.; Kubota, T.; Nakagawa, Y.; Tomishige, K. *ChemCatChem* **2010**, *2*, 547−555.
(30) Chia, M.; Pagán-Torres, Y. J.; Hibbitts, D.; Tan, Q.; Pham, H. N.; Datye, A. K.; Neurock, M.; Davis, R. J.; Dumesic, J. A. *J. Am. Chem. Soc.* **2011**, *133*, 12675−12689.
(31) Chen, K.; Mori, K.; Watanabe, H.; Nakagawa, Y.; Tomishige, K. *J. Catal.* **2012**, *294*, 171−183.
(32) Liu, S.; Amada, Y.; Tamura, M.; Nakagawa, Y.; Tomishige, K. *Green Chem.* **2014**, *16*, 617−626.
(33) Buntara, T.; Noel, S.; Phua, P. H.; Melián-Cabrera, I.; de Vries, J. G.; Heeres, H. J. *Angew. Chem., Int. Ed.* **2011**, *50*, 7083−7087.
(34) Buntara, T.; Noel, S.; Phua, P. H.; Melián-Cabrera, I.; de Vries, J. G.; Heeres, H. J. *Top. Catal.* **2012**, *55*, 612−619.
(35) Buntara, T.; Melián-Cabrera, I.; Tan, Q.; Fierro, J. L. G.; Neurock, M.; de Vries, J. G.; Heeres, H. J. *Catal. Today* **2013**, *210*, 106−116.
(36) Chatterjee, M.; Kawanami, H.; Ishizaka, T.; Sato, M.; Suzuki, T.; Suzuki, A. *Catal. Sci. Technol.* **2011**, *1*, 1466−1471.
(37) Seo, G.; Chon, H. *J. Catal.* **1981**, *67*, 424−429.
(38) Rodiansono, S.; Khairi, T.; Hara, T.; Ichikuni, N.; Shimazu, S. *Catal. Sci. Technol.* **2012**, *2*, 2139−2145.
(39) Sitthisa, S.; Resasco, D. E. *Catal. Lett.* **2011**, *141*, 784−791.
(40) Connolly, T. J.; Considine, J. L.; Ding, Z.; Fordatz, B.; Jennings, M. N.; MacEwan, M. F.; McCoy, K. M.; Place, D. W.; Sharma, A.; Sutherland, K. *Org. Process Res. Dev.* **2010**, *14*, 459−465.
(41) Nakagawa, Y.; Nakazawa, H.; Watanabe, H.; Tomishige, K. *ChemCatChem* **2012**, *4*, 1791−1797.
(42) Nakagawa, Y.; Tomishige, K. *Catal. Commun.* **2010**, *12*, 154−156.
(43) Merat, N.; Godawa, C.; Gaset, A. *J. Chem. Technol. Biotechnol.* **1990**, *48*, 145−159.
(44) Alamillo, R.; Tucker, M.; Chia, M.; Pagán-Torres, Y.; Dumesic, J. *Green Chem.* **2012**, *14*, 1413−1419.
(45) Biradar, N. S.; Hengne, A. M.; Birajdar, S. N.; Niphadkar, P. S.; Joshi, P. N.; Rode, C. V. *ACS Sustainable Chem. Eng.* **2014**, *2*, 272−281.
(46) Tuteja, J.; Choudhary, H.; Nishimura, S.; Ebitani, K. *ChemSusChem* **2014**, *7*, 96−100.
(47) Shiavo, V.; Descotes, G.; Mentech, J. *Bull. Soc. Chim. Fr.* **1991**, *128*, 704−711.
(48) Horvat, J.; Klaić, B.; Metelko, B.; Šunjić, V. *Tetrahedron Lett.* **1985**, *26*, 2111−2114.
(49) Patil, S. K. R.; Lund, C. R. F. *Energy Fuels* **2011**, *25*, 4745−4755.
(50) Ponec, V. *Appl. Catal., A* **1997**, *149*, 27−48.
(51) Mäki-Arvela, P.; Hájek, J.; Salmi, T.; Murzin, D. Y. *Appl. Catal., A* **2005**, *292*, 1−49.
(52) Lee, J.; Kim, Y. T.; Huber, G. W. *Green Chem.* **2014**, *16*, 708−718.
(53) Zou, W.; Gonzalez, R. D. *Catal. Lett.* **1992**, *12*, 73−86.
(54) Mahmoud, S.; Hammoudeh, A.; Gharaibeh, S.; Melsheimer, J. *J. Mol. Catal. A* **2002**, *178*, 161−167.
(55) Rocha, A. S.; Moreno, E. L.; da Silva, G. P. M.; Zotin, J. L.; Faro, A. C., Jr. *Catal. Today* **2008**, *133−135*, 394−399.
(56) López-De Jesús, Y. M.; Johnson, C. E.; Monnier, J. R.; Williams, C. T. *Top. Catal.* **2010**, *53*, 1132−1137.
(57) Ziaei-azad, H.; Yin, C.-X.; Shen, J.; Hu, Y.; Karpuzov, D.; Semagina, N. *J. Catal.* **2013**, *300*, 113−124.
(58) Nakagawa, Y.; Shinmi, Y.; Koso, S.; Tomishige, K. *J. Catal.* **2010**, *272*, 191−194.
(59) Amada, Y.; Shinmi, Y.; Koso, S.; Kubota, T.; Nakagawa, Y.; Tomishige, K. *Appl. Catal., B* **2011**, *105*, 117−127.
(60) Satsuma, A.; Osaki, K.; Yanagihara, M.; Ohyama, J.; Shimizu, K. *Appl. Catal., B* **2013**, *132−133*, 511−518.
(61) Hirasawa, S.; Watanabe, H.; Kizuka, T.; Nakagawa, Y.; Tomishige, K. *J. Catal.* **2013**, *300*, 205−216.
(62) Pang, S. H.; Medlin, J. W. *ACS Catal.* **2011**, *1*, 1272−1283.
(63) Vorotnikov, V.; Mpourmpakis, G.; Vlachos, D. G. *ACS Catal.* **2012**, *2*, 2496−2504.
(64) Sitthisa, S.; Sooknoi, T.; Ma, Y.; Balbuena, P. B.; Resasco, D. E. *J. Catal.* **2011**, *277*, 1−13.
(65) Sitthisa, S.; Pham, T.; Prasomsri, T.; Sooknoi, T.; Mallinson, R. G.; Resasco, D. E. *J. Catal.* **2011**, *280*, 17−27.
(66) Reyes, P.; Aguirre, M. C.; Melián-Cabrera, I.; López Granados, M.; Fierro, J. L. G. *J. Catal.* **2002**, *208*, 229−237.